AUTHOR QUERY FORM

ELSEVIER	**Journal:** EPSL **Article Number:** 12151	**Please e-mail or fax your responses and any corrections to:** **E-mail:** corrections.essd@elsevier.vtex.lt **Fax: +1 61 9699 6735**

Dear Author,

Please check your proof carefully and mark all corrections at the appropriate place in the proof (e.g., by using on-screen annotation in the PDF file) or compile them in a separate list. Note: if you opt to annotate the file with software other than Adobe Reader then please also highlight the appropriate place in the PDF file. To ensure fast publication of your paper please return your corrections within 48 hours.

For correction or revision of any artwork, please consult *http://www.elsevier.com/artworkinstructions*

Any queries or remarks that have arisen during the processing of your manuscript are listed below and highlighted by flags in the proof. Click on the 'Q' link to go to the location in the proof.

Location in article	**Query / Remark: click on the Q link to go** **Please insert your reply or correction at the corresponding line in the proof**
Q1, Q2	Please confirm that given names and surnames have been identified correctly and are presented in the desired order. (p. 1/ line 16,17)
Q3	Affiliation 'b' has been corrected. Please check, and amend if necessary. (p. 1/ line 19)
Q4, Q5	The resolution of Figures 2 and 3 is too low to be used. Please provide better quality figures. (p. 4/ line 45; p. 5/ line 51)
Q6, Q7	Figures 6 and 7 are not cited in the text. Please provide a citation for them. (p. 8/ line 36,120)
Q8, Q9	References given here were noted in the reference list but are missing from the text - please position each reference in the text or delete it from the list: Buesseler et al. (1992), Falkowski et al. (1991), Hung et al. (2007), Waples et al. (2006). (p. 11/ line 47,48)

Please check this box if you have no corrections to make to the PDF file ☐

Thank you for your assistance.

Contents lists available at ScienceDirect
Earth and Planetary Science Letters
www.elsevier.com/locate/epsl

Apparent enhancement of ^{234}Th-based particle export associated with anticyclonic eddies

Kuanbo Zhou[a], Minhan Dai[a,*], Shuh-Ji Kao[a], Lei Wang[a], Peng Xiu[b], Fei Chai[b], Jiwei Tian[c], Yang Liu[a]

[a] State Key Laboratory of Marine Environmental Science, Xiamen University, Xiamen 361005, China
[b] School of Marine Sciences, University of Maine, Orono, ME 04469, USA
[c] Physical Oceanography Laboratory, Ocean University of China, Qingdao 266003, China

ARTICLE INFO

Article history:
Received 27 September 2012
Received in revised form 23 May 2013
Accepted 27 July 2013
Available online xxxx
Editor: G. Henderson

Keywords:
anticyclonic eddy
thorium-234
particle export
submesoscale circulation
South China Sea

ABSTRACT

It is increasingly recognized that mesoscale eddies play an important role in modulating the variability of ocean biogeochemistry. It is commonly believed that contrary to cyclonic eddies, anticyclonic eddies are characterized by downwelling at their core regime, which may suppress particle export. Here, by considering submesoscale domains we demonstrate that particle export might be alternatively enhanced in anticyclonic eddies on the basis of a study carried out in the oligotrophic northern South China Sea basin. We examined particle fluxes associated with three coherent anticyclonic eddies using the naturally occurring radionuclide ^{234}Th. When applying a 1D steady-state model, ^{234}Th and its derived particulate organic carbon (POC) fluxes in all three eddy cores were 1.9- and 1.6-fold higher, respectively, relative to those in the non-eddy region. However, an eddy-resolving circulation numerical model showed complex submesoscale circulations associated with the anticyclonic eddy. Notably, dynamic interactions occurred at submesoscales that might induce advection into the eddy core from the edge, where the ^{234}Th deficit was elevated owing to higher particle production and export, probably stimulated by upwelling at the edges. We suggest therefore that enhanced particle fluxes derived from the 1D model along the vertical horizon at eddy cores only appeared to be changes, and that horizontal advection between the eddy core and edge should be taken into consideration in the flux estimation. Indeed, by integrating the ^{234}Th deficit among multiple profiles in the entire anticyclonic eddy system, we derived an average ^{234}Th flux of 938 $\text{dpm}\,\text{m}^{-2}\,\text{d}^{-1}$ at the 100-m horizon, equivalent to a POC flux of 3.69 $\text{mmol}\,\text{C}\,\text{m}^{-2}\,\text{d}^{-1}$. This export level was 1.6-fold higher than that from the reference sites.

1. Introduction

Mesoscale eddies are ubiquitous features in the ocean and it is increasingly recognized that they play an essential role in ocean biogeochemistry (Benitez-Nelson et al., 2007; Buesseler et al., 2008; Chelton et al., 2011; Klein and Lapeyre, 2009; McGillicuddy et al., 1998; Oschlies and Garcon, 1998). There are three types of eddy identified in the ocean: cyclonic, anticyclonic, and mode-water eddies (McGillicuddy et al., 2007). The current understanding is that cyclonic or cold eddies may induce nutrient injection from the depths into the euphotic zone associated with isopycnal uplift, which stimulates primary production (PP) and ultimately enhances the downward particle flux. By contrast, it is inferred that anticyclonic or warm eddies have a minor biogeochemical effect because of the general downward displacement of isopycnals therein (McGillicuddy et al., 1998). At the Bermuda Atlantic Time-series Study site (BATS, 31.83° N, 64.17° W), anticyclonic eddies even suppress spring blooms (Sweeney et al., 2003). Hansen et al. (2010) reported that algal blooms are delayed by ∼2 weeks owing to anticyclonic eddies in the Norwegian Sea. Moutin and Prieur (2012) showed that dissolved organic carbon (DOC) was higher in the upper 500 m of three anticyclonic eddies in the Mediterranean Sea than at non-eddy stations. Lasternas et al. (2012) attributed DOC accumulation to an increase in algal cell mortality and lysis rate in the early stage of anticyclonic eddy development in the Canary Eddy Corridor of the Northeast Atlantic Ocean. The authors suggested that such a DOC-enhanced microbial loop process would imply a reduction in the downward particulate organic carbon (POC) flux. A modeling study in the South China Sea (SCS) also showed that the export flux in anticyclonic eddies was 31% lower relative to the basin mean, in contrast to a 41% enhancement in cyclonic eddies (Xiu and Chai, 2011). However, it should be noted that the assessment of POC fluxes in the above mentioned studies were based on single station measurements, inferences, or

* Corresponding author. Tel.: +86 592 2182132; fax: +86 592 2184101.
E-mail address: mdai@xmu.edu.cn (M. Dai).

0012-821X/$ – see front matter
http://dx.doi.org/10.1016/j.epsl.2013.07.039

numerical modeling. Direct observations of POC fluxes with reasonably good spatial resolution have thus far been rare.

More importantly, no studies in light of the increasingly recognized submesoscale processes have been reported for POC export in anticyclonic eddies. We note that both observational and/or numerical modeling studies (although limited) have increasingly pointed towards the importance of considering submesoscale processes in resolving the biogeochemical impact of anticyclonic eddies. Indeed, small-scale hotspots of upwelling occur to the periphery of anticyclonic eddies, serving as a frontal zone between the eddy and the surrounding waters, owing to intensification of ageostrophic secondary circulation (Klein and Lapeyre, 2009). Model simulation further indicates that nutrient supply and PP can be alternatively stimulated by such submesoscale processes in anticyclonic eddies (Mahadevan et al., 2008). Samuelsen et al. (2012) used an eddy-resolving physical model with a particle-tracking module to show that particles tend to accumulate at the edge of an eddy.

Notwithstanding submesoscale processes, we contend that the inferred suppression of export fluxes by anticyclonic eddies should be re-examined by considering submesoscale processes. In this context, we conducted a study to examine the responses of particle export to three anticyclonic eddies using high-resolution sampling of ^{234}Th as an effective tracer. We compared ^{234}Th-derived export fluxes based on a 1D steady-state (SS) model and integrated fluxes at canceled the lateral variability induced by submesoscale transport. This comparison revealed that POC fluxes derived from the 1D model only appeared to be changes, and disappeared when a 3D model was applied, or that the vertical ^{234}Th fluxes estimated were biased by submesoscale lateral transport of ^{234}Th. We further introduced an eddy-resolving numerical model that revealed a 3D eddy structure to estimate the physical transport of ^{234}Th; this confirmed significant exchange between the eddy core and edge.

2. Methods

2.1. Study area

The SCS is the largest semi-enclosed marginal sea of the Pacific Ocean. The basin-scale circulation is mainly driven by the East Asian monsoon, which is expressed as a generally cyclonic gyre in winter and a two-gyre system in summer (Fig. 1a) comprising a cyclonic gyre north of approximately 12° N and an anticyclonic gyre in the south (Cao and Dai, 2011 and references therein). Eddies are frequently generated in the SCS owing to different mechanisms (Hu et al., 2011) such as frontal instability, coastal jet separation, and/or monsoon-driven forcing. In the northern SCS basin, eddies are mainly formed as a result of the variation and/or instability of these circulation gyres (Wang et al., 2003) or eddy penetration through the Kuroshio from the Western Pacific Ocean (Hu et al., 2012).

The SCS is an oligotrophic mini-ocean (Du et al., 2013) with PP in the range 16–46 mmol C m^{-2} d^{-1}; higher values usually occur in winter, when the mixed layer is deepened (Chen, 2005). Eddy activities are thus expected to be important for the biogeochemistry of the SCS basin. For example, PP could be elevated to >90 mmol C m^{-2} d^{-1} by a cyclonic eddy in the northern SCS (Chen et al., 2007). Lin et al. (2010) found that eddies can bring coastal nutrients into the oligotrophic basin and induce an algal bloom [chlorophyll (Chl) *a* concentration as high as 300–400 ng L^{-1}].

2.2. Sample collection

The sampling campaign was conducted from 28 July to 7 August 2007 on board the R/V *Dongfanghong II* in the northern SCS basin (Fig. 1b). Two transects were visited during the cruise: transect H along 18° N, covering all three of the anticyclonic eddies under study; and transect G along 19° N, located outside the eddies. Discrete water samples were collected at five depths in the upper 100 m (normally 0, 25, 50, 75, and 100 m) using 12-L Niskin bottles assembled on a CTD (Seabird SBE 911)/Rosette sampler. For the stations denoted in red in Fig. 1b, a small volume (4 L) of seawater was collected for total ^{234}Th determination and another 8 L was filtered on board using a quartz microfiber (QMA) filter (25 mm, 1.0 μm) for particulate ^{234}Th and POC analysis. Samples for biogenic SiO_2 (bSiO_2) analysis were collected only from selected stations (H06, H08, H10, H12, H14, H16, G04, G06, G08, and G10), for which 2 L of seawater was filtered through a 1.0-μm polycarbonate membrane filter. Nutrients were sampled only for stations denoted in black in Fig. 1b.

2.3. ^{234}Th analysis

We used the small-volume (4 L) MnO_2 co-precipitation method for total ^{234}Th analysis (Benitez-Nelson et al., 2001; Buesseler et al., 2001; Cai et al., 2006; Zhou et al., 2012). In brief, ^{234}Th was co-precipitated with MnO_2 formed by addition of $KMnO_4$ and $MnCl_2$ solutions, and was then filtered through a QMA filter (25 mm, 1.0 μm). ^{234}Th recovery was monitored by adding ∼10 dpm ^{230}Th. All total and particulate ^{234}Th samples were dried and mounted on plastic discs with two layers of aluminum foil (total density ∼7.2 mg m^{-2}) and one layer of Mylar film. A gas-flow proportional low-level RISØ beta counter was used for ^{234}Th counting. All ^{234}Th samples were counted for at least 12 h until 2500 counts were obtained. To determine the background, a second count was carried out after >6 months. Total ^{234}Th samples were demounted for recovery analysis of the ^{230}Th spike on QMA filters after beta counting. The ^{230}Th was monitored using ^{228}Th, purified using iron precipitation and anion column exchange, and finally plated on a 25-mm stainless steel disc. The disc samples were counted using an alpha counter until the counting errors for both ^{230}Th and ^{228}Th were <2%. All ^{230}Th recovery results lay between 78% and 101%, with an average of 89.6 ± 2.4% (mean ±1σ, $n = 85$). The ^{234}Th data presented here were calibrated after recovery and decay-corrected back to the sampling time. The uncertainties for ^{234}Th were propagated from counting errors associated with the first and second counts, recovery analysis, and the detection efficiency of the beta counter. The precision of the final ^{234}Th value was approximately 5%. On the basis of its conservative characteristics in the open ocean, the linear relationship ^{238}U (dpm L^{-1}) = 0.07081 × salinity was applied for estimating uranium activity (Chen et al., 1986). The uncertainty derived from this equation was approximately 3%, which was also included in the calculation of ^{234}Th fluxes.

2.4. POC and bSiO_2 analysis

The particulate ^{234}Th samples were used for POC measurements after beta counting. The QMA filters were fumed with concentrated HCl to remove carbonate. After drying in an oven at 50 °C, POC was determined using a PE-2400 SERIES II CHNS/O analyzer according to the JGOFS protocol (Knap et al., 1996). The procedural carbon blank was <0.06 μmol L^{-1} and the uncertainty for our POC data was better than 10%. bSiO_2 was measured using a Technicon AA3 auto-analyzer (Bran-Lube, GmbH) after double-wet alkaline (NaOH) digestion following Ragueneau et al. (2005) and Liu et al. (2012). The procedural blank for bSiO_2 was <0.03 μmol L^{-1} and the uncertainty was <10%. The uncertainties for both POC and bSiO_2 were considered during flux estimation.

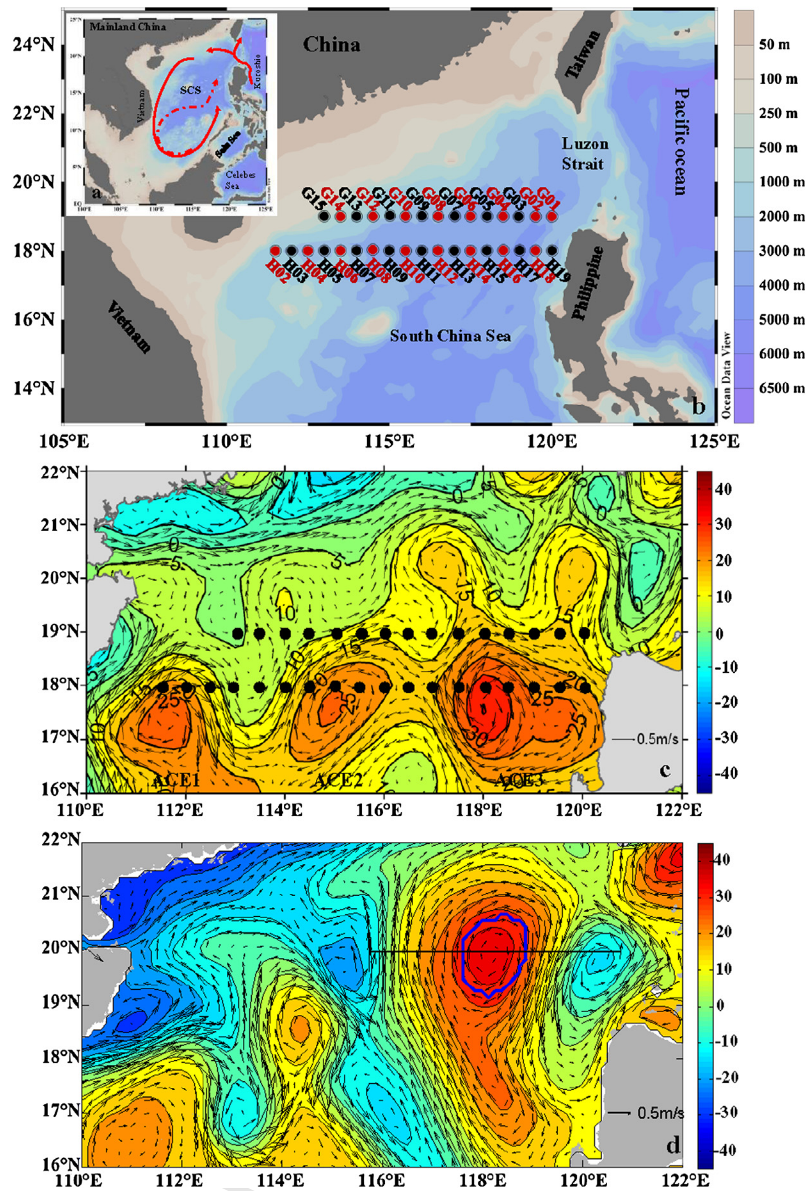

Fig. 1. (a) Map of the whole South China Sea (SCS) showing the basin-scale circulation [cyclonic in summer (solid line) and anticyclonic in winter (dashed line)] modified from Cao and Dai (2011). (b) The locations of sampling stations during the July–August 2007 cruise are shown as solid dots, and stations for ^{234}Th and nutrient analyses are marked in red and black, respectively. The bathymetry of the study area is also shown. (c) Map of sea-level anomalies (SLAs) and the derived surface geostrophic currents ($m\,s^{-1}$). The three anticyclonic eddies were marked by the elevated distribution of SLAs. From left to right, these eddies were denoted by ACE1, ACE2, and ACE3. The sampling stations are superimposed as solid black dots in the SLA map. (d) Modeled SLAs and surface geostrophic current on 4 July 2007. The blue contour denotes the boundary of the targeted anticyclonic eddy. One transect cutting through the eddy center (black line) was chosen to analyze the eddy structure (illustrated in Fig. 8).

2.5. Model description

We applied an eddy-resolving circulation model based on the Regional Ocean Model System. A detailed description of the model has been discussed by Xiu et al. (2010). In brief, the model domain covers the entire Pacific Ocean (45° S to 65° N, 99° E to 70° W) with realistic geometry and topography. In our case, we focused only on the northern SCS where in situ observations had been carried out. The horizontal resolution of the model is approximately 12.5 km in the SCS and it has 30 terrain-following vertical layers with intentionally enhanced resolution in the surface and bottom layers to better simulate upper ocean dynamics. This spacing can resolve mesoscale features and submesoscale features in the SCS region, which seem to be in accordance with satellite observations (Xiu et al., 2010).

3. Results

3.1. Eddy characterization

The positions of three anticyclonic eddies (ACE1, ACE2, and ACE3) during our observations were discernible from the sea-level anomaly (SLA) obtained from the Global Near-Real-Time SLA Data viewer at the University of Colorado (Fig. 1c). The maximum SLA for ACE3 during our observations was as high as 40 cm, compared to 30 cm for ACE1 and ACE2. The clockwise circulation of these surface geostrophic currents confirmed their anticyclonic characteristics. The evolutions of these eddies are described in the supplementary material.

As illustrated in Fig. 2, there was no obvious difference in hydrography between the three eddies, which is consistent with implication of the same source water during their formation (Nan et

Please cite this article in press as: K. Zhou et al., Apparent enhancement of ^{234}Th-based particle export associated with anticyclonic eddies, Earth Planet. Sci. Lett. (2013), http://dx.doi.org/10.1016/j.epsl.2013.07.039

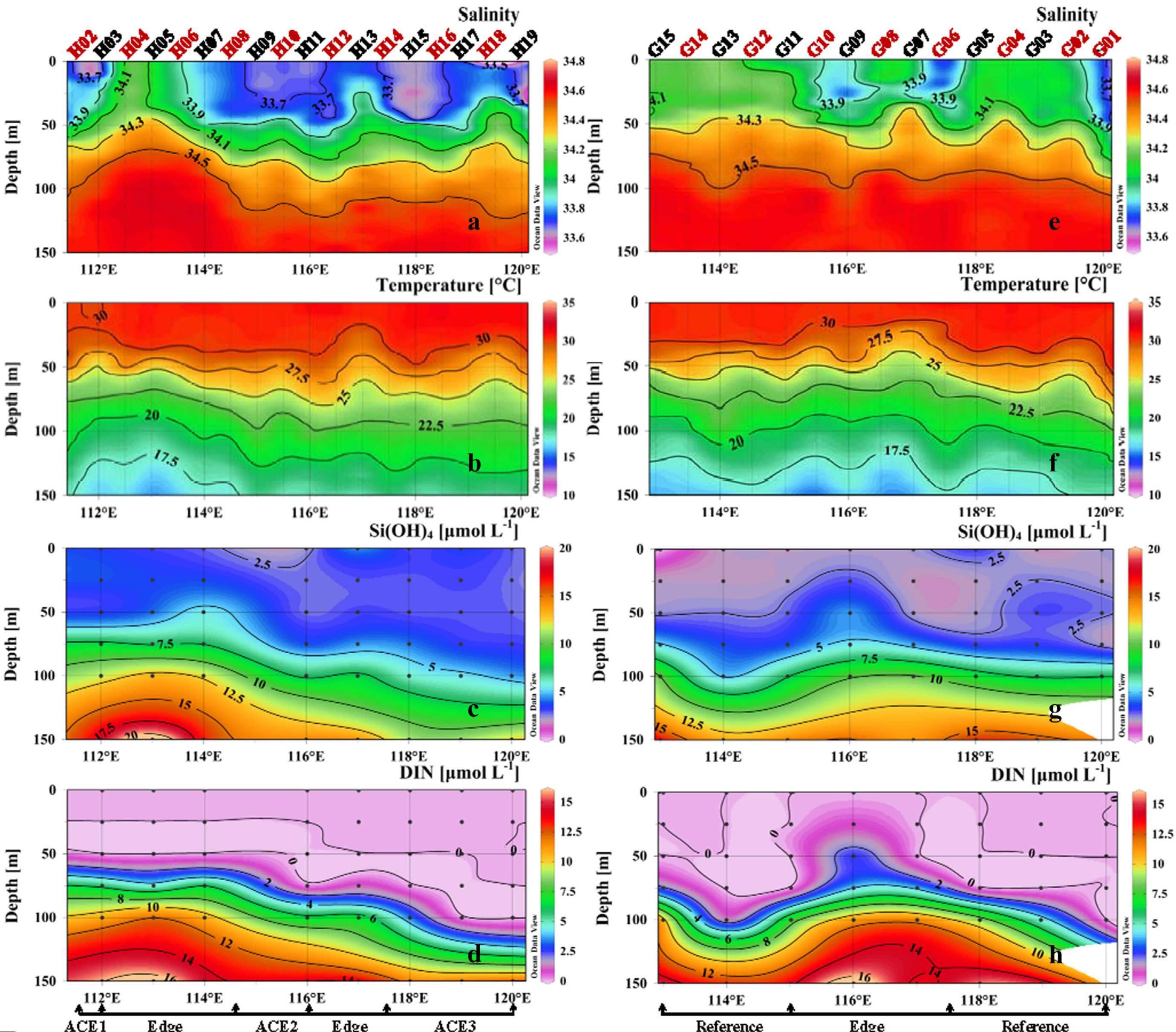

Fig. 2. Sectional distribution of the hydrography and nutrients in the upper 150 m. Distributions of (a) salinity, (b) temperature, (c) $Si(OH)_4$, and (d) DIN along transect H, and of (e) salinity, (f) temperature, (g) $Si(OH)_4$, and (h) DIN along transect G. The stations are denoted at the top and separated into ACE1, ACE2, ACE3, eddy edges, and reference stations at the bottom.

al., 2011). They were characterized by lower salinity ($S < 33.7$) at the surface relative to the surrounding waters ($S > 34$). The water was well mixed in the upper 25 m, and downward displacement of both isohaline and isothermal water began to emerge at a depth of 50 m; for example, the temperature in the eddy centers was 27.5 °C compared to 25 °C for the reference stations. In addition, the isohaline water seemed to be uplifted at the eddy edges; for example, the salinity at stations H04, H05, and H12 was >33.9 but was <33.7 in the eddy cores.

The distribution of dissolved nutrients is also shown in Fig. 2. As expected, their concentrations were very low in the surface water of the eddies. For example, the DIN concentration was below the detection limit within the upper 50 m in the core of both ACE2 and ACE3. It became measurable at 100 m, where it was ~6.0 μmol L^{-1} in ACE2 and 0–4 μmol L^{-1} in ACE3.

It was not surprising that similar dissolved inorganic nitrogen (DIN) concentrations were observed in the surrounding waters, where surface salinity was >34. One interesting finding was that the DIN concentration was enhanced at stations at the eddy edges; for example, the DIN concentration at 100 m was 7–12 μmol L^{-1} at the peripheries compared to 0–6 μmol L^{-1} within the eddy cores (Fig. 2d). The distribution of Chl *a* in transects H and G is presented in Fig. 3a, f. Consistent with previous studies (Liu et al., 2002), Chl *a* values were very low (<100 ng L^{-1}) in the upper 25 m and reached a maximum at ~75 m (known as the subsurface chlorophyll maximum, SCM). At the surface, Chl *a* did not differ between the eddies and ambient water. At the SCM, the Chl *a* concentration in the eddy cores varied from 130 to 240 ng L^{-1}, which was comparable to that at the reference stations (80–230 ng L^{-1}). However, concentrations were significantly higher at the eddy edges, ranging from 240 to 390 ng L^{-1}. Chl *a* profiles (Fig. 4) exhibited a similar distribution pattern between the eddy cores and ambient water, but differed at the edges (especially in the SCM layer).

Please cite this article in press as: K. Zhou et al., Apparent enhancement of ^{234}Th-based particle export associated with anticyclonic eddies, Earth Planet. Sci. Lett. (2013), http://dx.doi.org/10.1016/j.epsl.2013.07.039

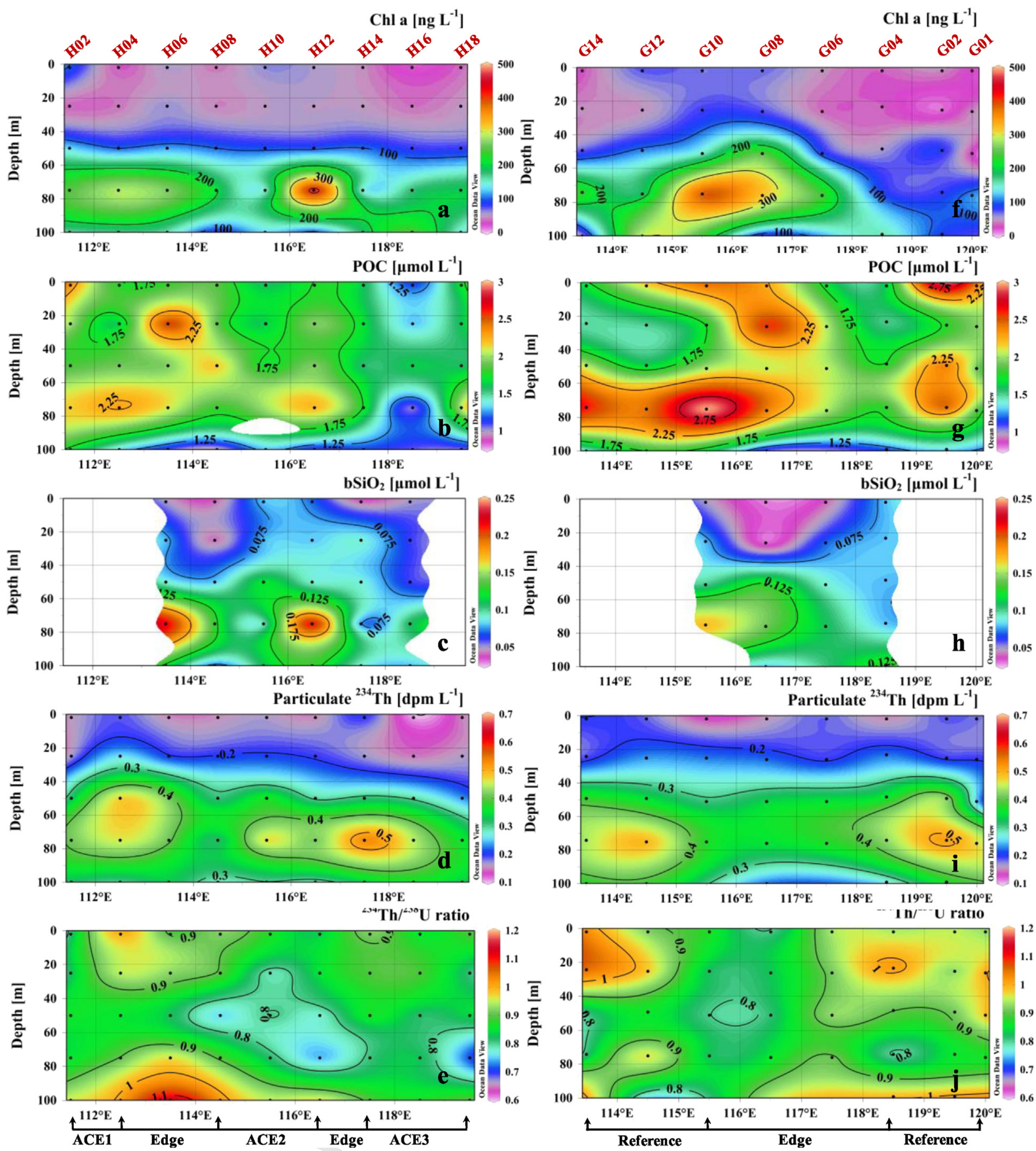

Fig. 3. Sectional distributions of (a, f) Chl *a*, (b, g) POC, (c, h) bSiO$_2$, (d, i) particulate ^{234}Th, and (e, j) ^{234}Th/^{238}U ratio. The left and right panels are distributions for transects H and G, respectively. The stations are denoted at the top and separated into ACE1, ACE2, ACE3, eddy edges, and references at the bottom.

On the basis of the SLA, hydrography, and Chl *a* in the SCM, our core sampling stations could be grouped into three water types (eddy core, eddy edge, and reference sites) according to principal analysis and *K*-means cluster analysis. The computation was carried out using the statistical software R (http://cran.r-project.org/mirrors.html) and the results are shown in supplementary Tables S4 and S5. According to the statistics, stations H02, H08, H10, H14, H16, and H18 represented eddy core water; eddy edge water came from stations H04, H06, H12, G06, G08, and G10; and the reference sites included stations H05, G01, G02, G04, G12, and G14.

3.2. POC and bSiO$_2$

bSiO$_2$ and POC distributions are shown in Fig. 3. The bSiO$_2$ concentration varied substantially from <0.1 to 0.22 μmol Si L^{-1} in the upper 100 m. In the SCM layer, the bSiO$_2$ concentration ranged from 0.11 to 0.22 μmol Si L^{-1} at the eddy edges, and was up to twice as high as in the eddy core and reference stations (0.09–0.13 μmol Si L^{-1}).

POC concentrations ranged between 1.0 and 3.0 μmol C L^{-1} in the upper 100 m. In the upper 25 m, the POC concentration was high (1.50–2.86 μmol C L^{-1}) but did not differ among the three water types. In the SCM layer, similar enhancement was evident

Please cite this article in press as: K. Zhou et al., Apparent enhancement of ^{234}Th-based particle export associated with anticyclonic eddies, Earth Planet. Sci. Lett. (2013), http://dx.doi.org/10.1016/j.epsl.2013.07.039

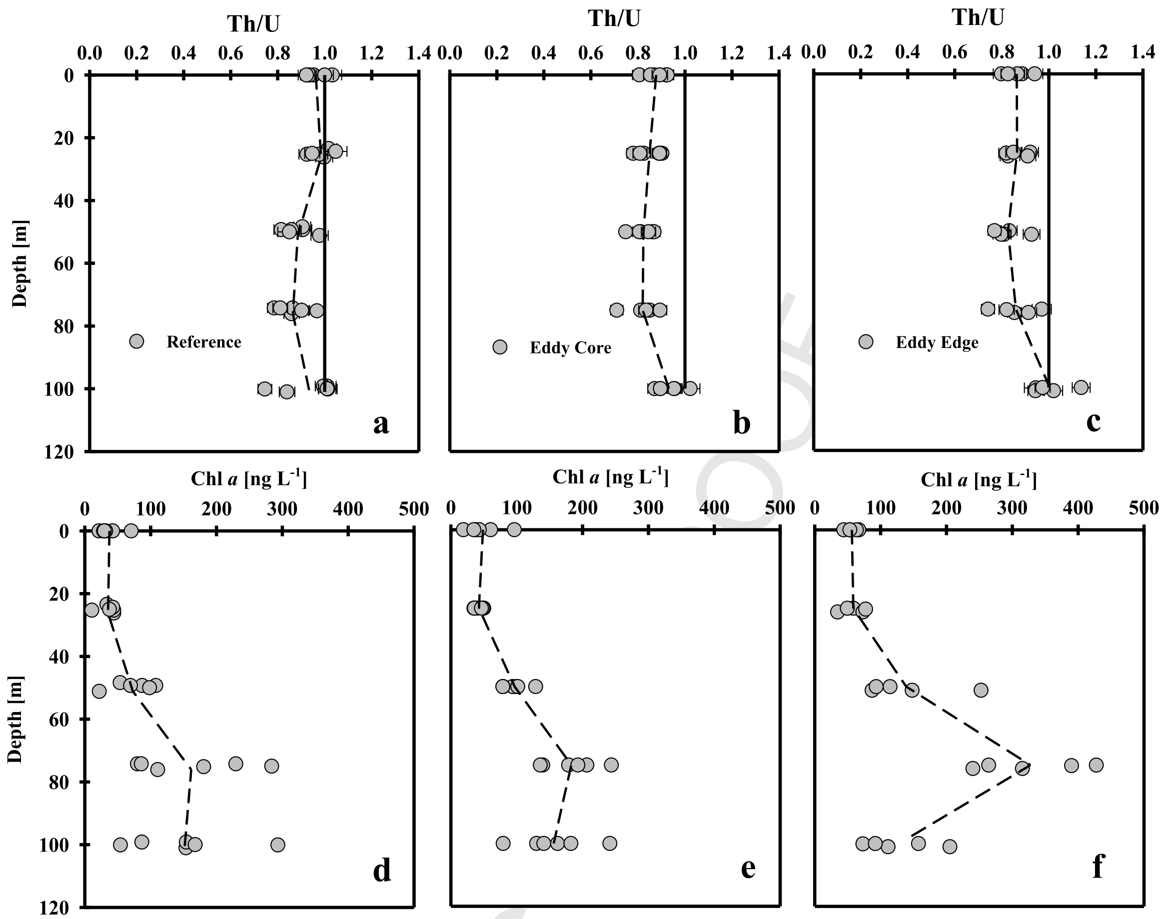

Fig. 4. Vertical profiles of $^{234}Th/^{238}U$ (upper panel) and Chl *a* (lower panel) in the upper 100 m for (a, d) reference stations, (b, e) eddy cores, and (c, f) eddy edges. The dashed lines show profiles of the average values.

at the eddy edge stations (2.07–3.00 μmol C L^{-1} at the edge vs. 1.64–2.18 μmol C L^{-1} in the eddy core).

3.3. ^{234}Th distribution

We observed similar ^{234}Th variations in the upper 100 m compared to previous measurements in the region (Cai et al., 2008; Chen, 2008). Total ^{234}Th activity ranged between 1.73 ± 0.06 and 2.79 ± 0.06 dpm L^{-1}. Particulate ^{234}Th accounted for only 5–25% of the total ^{234}Th, at 0.10 ± 0.01 to 0.53 ± 0.004 dpm L^{-1}. At the reference stations, the ^{234}Th activity could be 92–105% of ^{238}U ($\sim$2.40 dpm L^{-1}) in the surface water, which indicates low ^{234}Th removal associated with particle export. Beneath the surface in the SCM layer, total ^{234}Th was lower, ranging from 2.00 ± 0.08 to 2.10 ± 0.09 dpm L^{-1}, and reached equilibrium with ^{238}U at a depth of 100 m. Such a distribution pattern has been described for other oligotrophic oceans (Cai et al., 2008; Coale and Bruland, 1987). In the eddy cores, ^{234}Th activity was lower, although the vertical profile showed similar trends. It ranged from 1.86 ± 0.06 to 2.21 ± 0.06 dpm L^{-1} at the surface, and from 1.73 ± 0.06 to 2.07 ± 0.07 dpm L^{-1} in the SCM layer, and similarly equilibrated with ^{238}U at 100 m. At the edge stations, total ^{234}Th varied from 1.92 ± 0.08 to 2.24 ± 0.08 dpm L^{-1} at the surface, but larger variation was found in the SCM layer (from 1.80 ± 0.07 to 2.22 ± 0.08 dpm L^{-1}). Particulate ^{234}Th activity (0.1–0.2 dpm L^{-1}) was low at the surface and exhibited a subsurface maximum of 0.4–0.5 dpm L^{-1} at a depth related to the SCM layer. However, particulate ^{234}Th activity did not seem to be well correlated with Chl *a* ($R^2 = 0.35$, Supplementary Fig. S2). In the SCM layer, particulate ^{234}Th activity at the eddy edge was comparable to that for the eddy cores and reference stations, while Chl *a* was much higher at the edge.

To further compare differences in total ^{234}Th among the three water types, profiles of the $^{234}Th/^{238}U$ ratio are shown in Fig. 4. The average $^{234}Th/^{238}U$ profile for the reference stations is closer to the line of unity compared to profiles for the eddy cores and edges. However, this difference in $^{234}Th/^{238}U$ profile between eddies and reference regimes was not reflected in Chl *a*, as discussed above.

3.4. ^{234}Th fluxes based on the 1D SS model

Assuming SS and no horizontal ^{234}Th transport, the ^{234}Th flux from the upper 100 m can be estimated according to the following equation, which has commonly been used in previous studies:

$$P_{Th} = \lambda_{Th} \int_0^{100} (A_U - A_{Th})\, dz, \qquad (1)$$

where P_{Th} is the ^{234}Th export flux, A_U and A_{Th} are ^{238}U and total ^{234}Th activities, and λ_{Th} is the ^{234}Th decay constant (0.02876 d^{-1}). ^{234}Th fluxes were calculated as 427 ± 114 to 1251 ± 100 dpm $m^{-2} d^{-1}$ ($n = 17$). For the reference stations, the ^{234}Th flux derived for the depth horizon of 100 m was very low, ranging from 464 ± 110 to 618 ± 111 dpm $m^{-2} d^{-1}$, with an average of 535 ± 53 dpm $m^{-2} d^{-1}$ (mean $\pm 1\sigma$, $n = 6$). In the eddy cores, the flux ranged from 800 ± 102 to 1251 ± 100 dpm $m^{-2} d^{-1}$, with an average of 1007 ± 29 dpm $m^{-2} d^{-1}$ ($n = 6$). At the

Please cite this article in press as: K. Zhou et al., Apparent enhancement of ^{234}Th-based particle export associated with anticyclonic eddies, Earth Planet. Sci. Lett. (2013), http://dx.doi.org/10.1016/j.epsl.2013.07.039

Table 1
Responses of particle export in eddy cores and eddy edges, and their comparisons with the reference stations outside the eddies.

Parameter	Reference ($n = 6$)	Eddy core[a] ($n = 6$)	Eddy edge[a] ($n = 5$)	Core + edge[a] ($n = 11$)	EC/R[b]	EE/R[b]	(EC + EE)/R
C/Th ratio @ 100 m (mmol C dpm^{-1})	4.41 ± 0.69	3.77 ± 0.90	4.13 ± 0.88	3.93 ± 0.87	0.9 (0.20)	0.9 (0.58)	0.89
Si/Th ratio @ 100 m (mmol Si dpm^{-1})	0.37 ± 0.10	0.30 ± 0.07	0.40 ± 0.12	0.34 ± 0.11	0.8	1.1	0.92
SS 1D ^{234}Th flux @ 100 m (dpm m^{-2} d^{-1})	535 ± 53	1007 ± 161	856 ± 393	938 ± 284	1.9 (0.005)	1.6 (0.14)	1.8
1D POC export @ 100 m (mmol C m^{-2} d^{-1})	2.35 ± 0.34	3.78 ± 1.03	3.47 ± 1.55	3.69 ± 1.38	1.6 (0.018)	1.5 (0.19)	1.6
1D bSiO$_2$ export @ 100 m[c] (mmol Si m^{-2} d^{-1})	0.20 ± 0.07	0.30 ± 0.09	0.38 ± 0.25	0.32 ± 0.15	1.5	1.9	1.6
3D/1D ^{234}Th flux ratio[d]	n.d.	0.50	n.d.	–	–	–	–
3D/1D POC flux ratio	n.d.	0.51	n.d.	–	–	–	–

[a] The values stand for mean ±1σ standard deviation.
[b] EC, EE, and R refer to Eddy Core, Eddy Edge, and Reference; The values in parentheses are the P results from simple t-tests for eddy cores vs. reference stations and eddy edges vs. reference stations assuming $\alpha = 0.05$.
[c] The station numbers of bSiO$_2$ for reference stations, eddy cores, and eddy edges are 1, 4, and 5. t-tests were not carried out for bSiO$_2$ owing to the limited sampling stations.
[d] “1D” and “3D” mean the fluxes without and with the consideration of advection between eddy core and eddy edge (based on the model-derived circulation scheme).

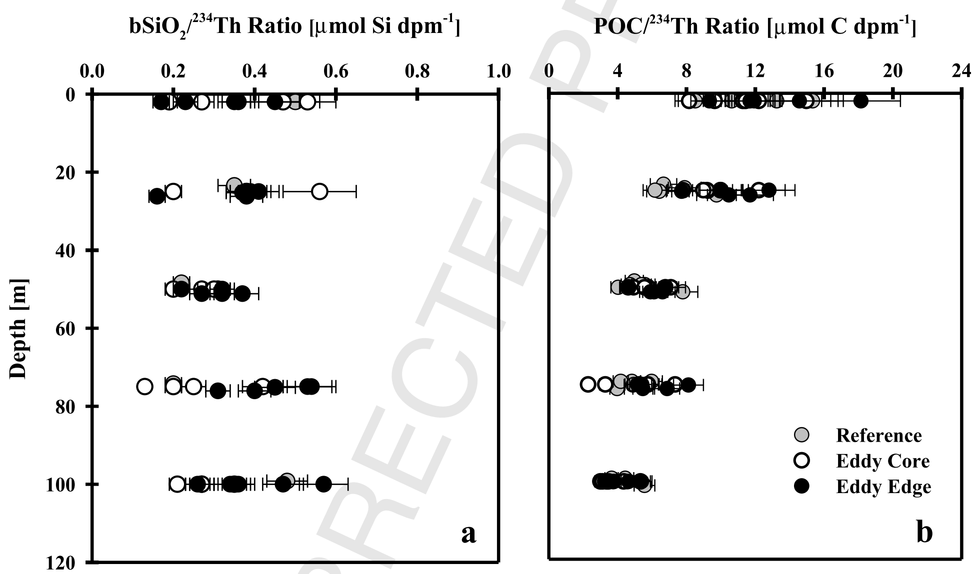

Fig. 5. Profiles of (a) bottle POC/^{234}Th and (b) bSiO$_2$/^{234}Th ratios in the upper 100 m for the reference, eddy core, and eddy edge stations.

eddy edges, greater variation in the ^{234}Th flux was observed, ranging from 427 ± 114 to 1239 ± 101 dpm m^{-2} d^{-1} (average 856 ± 36 dpm m^{-2} d^{-1}, $n = 5$). The ^{234}Th flux in the eddy cores was approximately two times higher than that for the reference stations (Table 1).

3.5. Profiles of bottle POC/^{234}Th and bSiO$_2$/^{234}Th ratios

Profiles of bottle POC/^{234}Th and bSiO$_2$/^{234}Th ratios are presented in Fig. 5. In general, the POC/^{234}Th ratio gradually decreased with depth, which is believed to be associated with preferential remineralization of organic carbon (Buesseler et al., 2006). In addition, the POC/^{234}Th ratio showed greater variation at the surface (8.16–18.15 μmol C dpm^{-1}) than at 100 m (3.0–5.6 μmol C dpm^{-1}). bSiO$_2$/^{234}Th exhibited a substantially different pattern. No significant depth-related variation in bSiO$_2$/^{234}Th ratio was observed for any station; the range was 0.17–0.53 μmol Si dpm^{-1} at the surface and 0.21–0.57 μmol Si dpm^{-1} at 100 m. This implies that bSiO$_2$ dissolution was not obvious compared to POC, as it represents the hard part of marine organisms (mostly diatom frustules). Note that the variation in bSiO$_2$/^{234}Th ratio between stations was 0.21–0.57 mmol Si dpm^{-1}, which is approximately 1.5-fold higher than for the POC/^{234}Th ratio (3.00–5.56 mmol C dpm^{-1}). At a depth of 100 m, the ratio varied from 3.65 ± 0.39 to 5.56 ± 0.60 μmol C dpm^{-1} for the reference stations, from 3.00 ± 0.32 to 5.33 ± 0.58 μmol C dpm^{-1} for the eddy cores, and from 3.24 ± 0.35 to 5.40 ± 0.59 μmol C dpm^{-1} for the edges. The differences in POC/^{234}Th ratio between the three water types were nonsignificant according to a simple t-test ($\alpha = 0.05$): $P = 0.20$ for eddy cores versus reference stations and $P = 0.58$ for eddy edges versus reference stations. The bottle bSiO$_2$/^{234}Th ratio was 0.48 ± 0.05 μmol Si dpm^{-1} for the reference stations (only station G04 was sampled), 0.21 ± 0.02 to 0.35 ± 0.04 μmol Si dpm^{-1} for the eddy cores, and 0.26 ± 0.03 to 0.57 ± 0.06 μmol Si dpm^{-1} for the edges. No statistical analysis of differences in bSiO$_2$/^{234}Th ratio among the water types was performed because only one reference station was covered.

4. Discussion

4.1. POC (bSiO$_2$)/^{234}Th and fluxes derived from the 1D SS model

To convert a ^{234}Th flux into POC and/or bSiO$_2$ flux, measurements of the POC/^{234}Th and/or bSiO$_2$/^{234}Th ratio for sinking particles are required. In the present study, only bottle POC/^{234}Th and bSiO$_2$/^{234}Th ratios were available for the export horizon of 100 m.

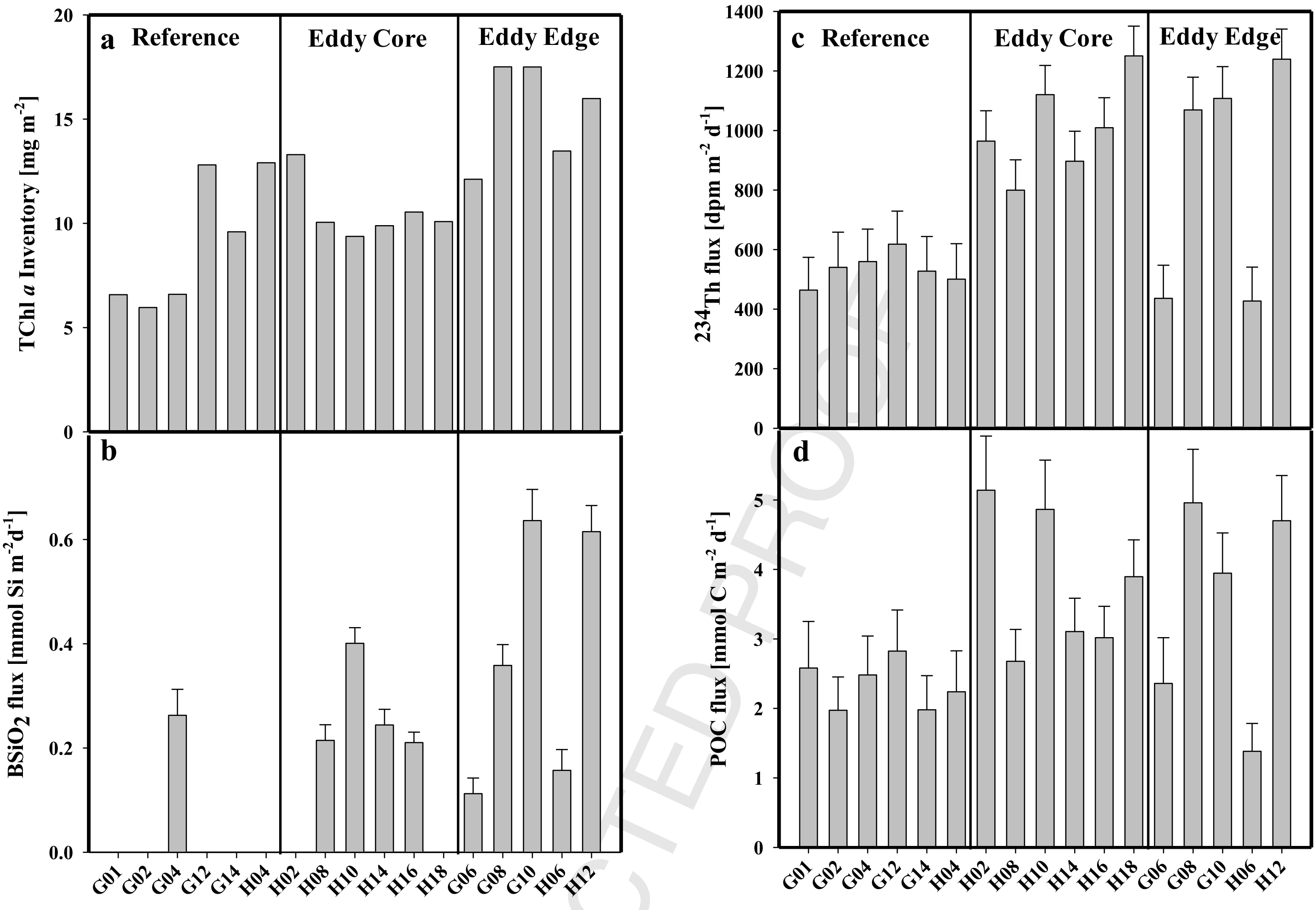

Q6 **Fig. 6.** Spatial distribution of (a) the Chl *a* inventory from 0 to 100 m, (b) $bSiO_2$ fluxes at 100 m, (c) ^{234}Th flux at 100 m, and (d) POC fluxes at 100 m. All stations were separated into reference, eddy cores, and eddy edges.

Although the POC/^{234}Th ratio for large particles is thought to be more representative for the truly sinking POC/^{234}Th ratio, the bottle POC/^{234}Th ratio is useful as an upper limit of the POC/^{234}Th ratio for sinking particles (Cai et al., 2010; Zhou et al., 2012). In previous studies carried out in the SCS basin, bottle POC/^{234}Th ratios were consistently higher than for large particles, but within twice the ratio for particles >53 μm (Chen, 2008). It has been suggested that the elevated POC/^{234}Th ratio for bottle filtrates may be induced by DOC adsorption and/or preferential capture of living zooplankton with elevated POC/^{234}Th ratios (Buesseler et al., 2006; Cai et al., 2008). In addition, bottle filtration allows sampling at higher resolution. At 100 m, bottle POC/^{234}Th ratios ranged between 3.0 ± 0.32 and 5.6 ± 0.60 μmol C dpm^{-1}. These ratios were within the range previously determined in the SCS (Cai et al., 2008; Chen, 2008).

Relative to bottle POC/^{234}Th, the influence of adsorption from the dissolved phase and/or zooplankton might be minor for the $bSiO_2$/^{234}Th ratio. In the present study, the bottle $bSiO_2$/^{234}Th ratio at 100 m ranged from 0.21 ± 0.02 to 0.57 ± 0.06 μmol Si dpm^{-1}. These values agree well with those for particles >53 μm determined in other oligotrophic oceans (Buesseler et al., 2008; Maiti et al., 2008), such as 0.10–0.33 μmol Si dpm^{-1} in the subtropical Pacific Ocean and 0.11–0.35 μmol Si dpm^{-1} in the North Atlantic Ocean. Multiplication of the ^{234}Th flux based on the 1D SS model by the POC/^{234}Th ($bSiO_2$/^{234}Th) ratio yielded their export fluxes. The POC fluxes derived for all stations ranged from 1.38 ± 0.40 to 5.14 ± 0.78 mmol C m^{-2} d^{-1} (supplementary Table S2). As expected, POC fluxes were low for the reference stations, ranging

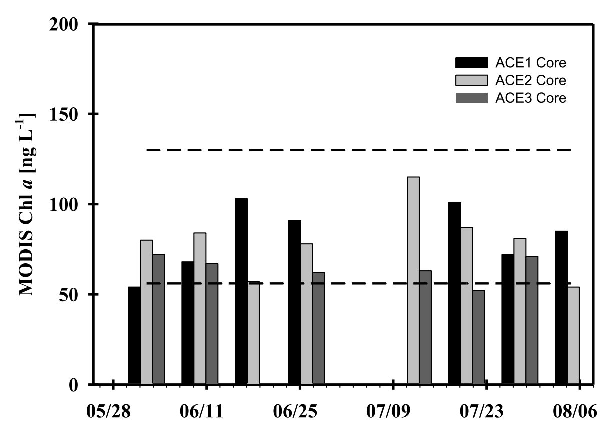

Fig. 7. Weekly composite of remotely sensed Chl *a* in three eddy cores (ACE1, ACE2, and ACE3) from the satellite MODIS during 25 May–5 August 2007. The two dashed lines denote the Chl *a* concentration range in the non-eddy region, which is the average satellite Chl *a* concentrations in an area of 36 km × 36 km centered at 113° E, 19° N. Q7

from 1.97 ± 0.48 to 2.83 ± 0.59 mmol C m^{-2} d^{-1} with an average of 2.35 ± 0.34 mmol C m^{-2} d^{-1}. Higher fluxes were found for the eddy cores, ranging from 2.68 ± 0.46 to 5.14 ± 0.78 mmol C m^{-2} d^{-1} with an average of 3.78 ± 1.03 mmol C m^{-2} d^{-1}. However, the POC fluxes observed at the edges were variable, ranging from 1.38 ± 0.40 to 4.97 ± 0.77 mmol C m^{-2} d^{-1} with an average of 3.47 ± 1.55 mmol C m^{-2} d^{-1}.

Please cite this article in press as: K. Zhou et al., Apparent enhancement of ^{234}Th-based particle export associated with anticyclonic eddies, Earth Planet. Sci. Lett. (2013), http://dx.doi.org/10.1016/j.epsl.2013.07.039

$bSiO_2$ fluxes were also estimated as 0.11 ± 0.03 to 0.64 ± 0.06 mmol Si m^{-2} d^{-1}. To the best of our knowledge, this is the first data set of $bSiO_2$ fluxes ever measured in the upper ocean within the SCS basin. $bSiO_2$ fluxes ranged from 0.21 ± 0.03 to 0.40 ± 0.03 mmol Si m^{-2} d^{-1} (average 0.27 ± 0.09 mmol Si m^{-2} d^{-1}, $n = 4$) in the eddy cores, and from 0.11 ± 0.03 to 0.64 ± 0.06 mmol Si m^{-2} d^{-1} (average 0.38 ± 0.25 mmol Si m^{-2} d^{-1}) at the edges, compared to 0.26 ± 0.05 mmol Si m^{-2} d^{-1} for the reference station.

In summary, the 1D model-based ^{234}Th and POC fluxes all appeared to be enhanced in the eddy cores, at 1.9- and 1.6-fold higher than for the reference stations (Table 1). According to t-tests, this enhancement was statistically significant within the 95% confidence interval ($P = 0.0048$ and 0.018). For the eddy edges, ^{234}Th and POC fluxes were 1.6- and 1.5-fold higher, respectively, than for the reference stations. However, statistical analysis indicated that the elevation of particle fluxes might not be significant at the edges ($P > 0.05$, values shown in Table 1). The large variation in particle fluxes at the edges might reflect the fact that the eddy edge usually acts as a frontal zone between the eddy core and ambient water with high biogeochemical dynamics. Resplandy et al. (2012) pointed out the assumption of 1D SS may induce large uncertainties for flux estimation when the spatial scale is of the order of 100 km, such as for mesoscale eddies. Moreover, the elevated ^{234}Th flux based on the 1D SS model and the derived POC flux for the eddy cores did not seem to be supported by the low nutrient loads, low Chl a, and picoplankton-dominated community structures (see the supplementary material).

4.2. Why the derived particle export was apparently enhanced in the eddy cores

The above discussion led us to examine if the assumption of 1D SS for deriving ^{234}Th and POC fluxes is valid for eddy systems and if the ^{234}Th flux contributed by lateral transport should be taken into consideration. Although a 3D physical structure of the entire anticyclonic eddy was not available, a physical model could help in simulating the dynamics of the anticyclonic eddies. Fig. 8 shows both the instantaneous and composite current fields and the potential vorticity (PV) within one of the anticyclonic eddies. Note that the model-derived physical structures were similar for all three eddies.

According to Fig. 8, it is probable that in terms of current fields during the early stage on 2 July 2007, the upward instant velocity (2–6 m d^{-1}) could have occurred at the peripheries of the eddy, while downward velocity (0–2 m d^{-1}) usually occurred at the center. This was also true if we considered the composite velocity for the whole lifespan of the eddy. The upwelling at the peripheries of the eddy might have been induced by ageostrophic secondary circulation (Mahadevan et al., 2008; Klein and Lapeyre, 2009). The elevated nutrients and total Chl a and the abundance of diatoms observed at the edges might be attributable to such upwelling (supplementary Table S3). The upwelled water could then have been transported inwards at the surface, as indicated by the horizontal velocity. However, water transport might have a large temporal variation. As shown in Fig. 8, the instantaneous velocity for inward transport could be >0.1 m s^{-1} when the eddy was in the early stage. However, the composite velocity was one order of magnitude lower. We could have expected that such inward transport would become weaker when the eddy stabilized and/or decayed. The PV distribution also supports such water transport. The vertical PV distribution was usually high at the surface and decreased with depth. Both instantaneous and composite PV isopleths were overall parallel with isopycnals at the surface, which implies that water parcels could move freely along density surfaces between the eddy core and edge (Olson, 1980).

It should be pointed out that Xiu et al. (2010) validated the eddy-resolving circulation model used here with satellite data. Further examination of the modeled SLAs and geostrophic currents during similar dates to our observations was also carried out in the model (Fig. 1c, d) and showed very similar anticyclonic eddies in the same region. Their SLAs in the eddy cores from left to right were >25, 25, and 35 cm, respectively, and the geostrophic currents at the edges were all >5 m s^{-1}, which are similar to those observed from the satellite data. This suggests that the physical model was robust enough to reproduce upper ocean dynamics observed in this region. In addition, the values lie well within the statistical range for modeled and observed eddies (Xiu et al., 2010), indicating that ACE1, ACE2, and ACE3 were typical mesoscale features in the SCS.

Because of the existence of inward transport, the 1D model assumption for estimating the ^{234}Th flux might not be valid. However, owing to the reliability of our physical model, the derived results could be applied to calculate horizontal ^{234}Th transport. Using a first-order estimation, ^{234}Th transport flux can be calculated according to

$$P_{core} = \lambda(A_U - A_{core}) + u\frac{A_{edge} - A_{core}}{\Delta x}, \qquad (2)$$

where P_{core} is the ^{234}Th flux in the eddy core during observation, A_{core} and A_{edge} are ^{234}Th activity before horizontal transport occurred, u is the horizontal transport velocity, and Δx is the distance between the core and edge. Since the horizontal transport velocity varied with eddy evolution, it is more reasonable to use the composite velocity for inward transport compared to the instantaneous velocity during our observations.

If we assume $P_{core} = 1007 \pm 161$ dpm m^{-2} d^{-1} (Table 1), $A_{edge} = (210.8 \pm 5.9) \times 10^3$ dpm m^{-2} as the average ^{234}Th activity in the upper 100 m (assuming the ^{234}Th activity was relatively stable at the eddy edge), $\Delta x = 60$ km, and $u = 0.03$ m s^{-1} as the composite velocity for inward transport, then A_{core} in the upper 100 m can be calculated as $(222.4 \pm 5.1) \times 10^3$ dpm m^{-2}. The "true" ^{234}Th flux in the eddy core after subtraction of horizontal transport is 506 ± 250 dpm m^{-2} d^{-1}, which is similar to flux for the reference stations (535 dpm m^{-2} d^{-1}).

We noted that the SS scenario seems to be applicable in this study. It is known that ^{234}Th can "remember" export events that occurred >100 days before sampling. Any algal blooms and subsequent high particle export during that time interval would elevate the ^{234}Th flux. Therefore, we tracked the distribution of surface Chl a from remote sensing data back to a time before the formation of the three eddies and extracted the Chl a concentration in the eddy cores identified by the SLA maps (supplementary Fig. S3 compares satellite and field-derived Chl a). The weekly composite of surface Chl a at the three eddy cores from 25 May to 5 August 2007 is shown in Fig. 9. Surface Chl a ranges in the three eddy cores were 54–103, 54–115, and 52–72 ng L^{-1}, compared to 56–130 ng L^{-1} for the reference stations, which suggests low Chl a and non-bloom conditions. It is evident that temporal variations in surface Chl a were similar between eddy cores and reference stations, where SS ^{234}Th fluxes were 535 dpm m^{-2} d^{-1}. Savoye et al. (2006) pointed out that SS should be applicable when SS ^{234}Th fluxes are <800 dpm m^{-2} d^{-1}. If we assume that the variation in surface Chl a is representative of the whole upper ocean (0–100 m), then the ^{234}Th flux induced by temporal variation should be identical between the eddy cores and the reference stations. In other words, we ruled out the non-SS scenario for the time scale of our observations.

Therefore, it is very likely that horizontal transport could have induced elevated particle export in the eddy cores. Moreover, if we add the eddy core and edge together, the average integrated ^{234}Th flux would be 938 ± 284 dpm m^{-2} d^{-1}, which is equivalent to a

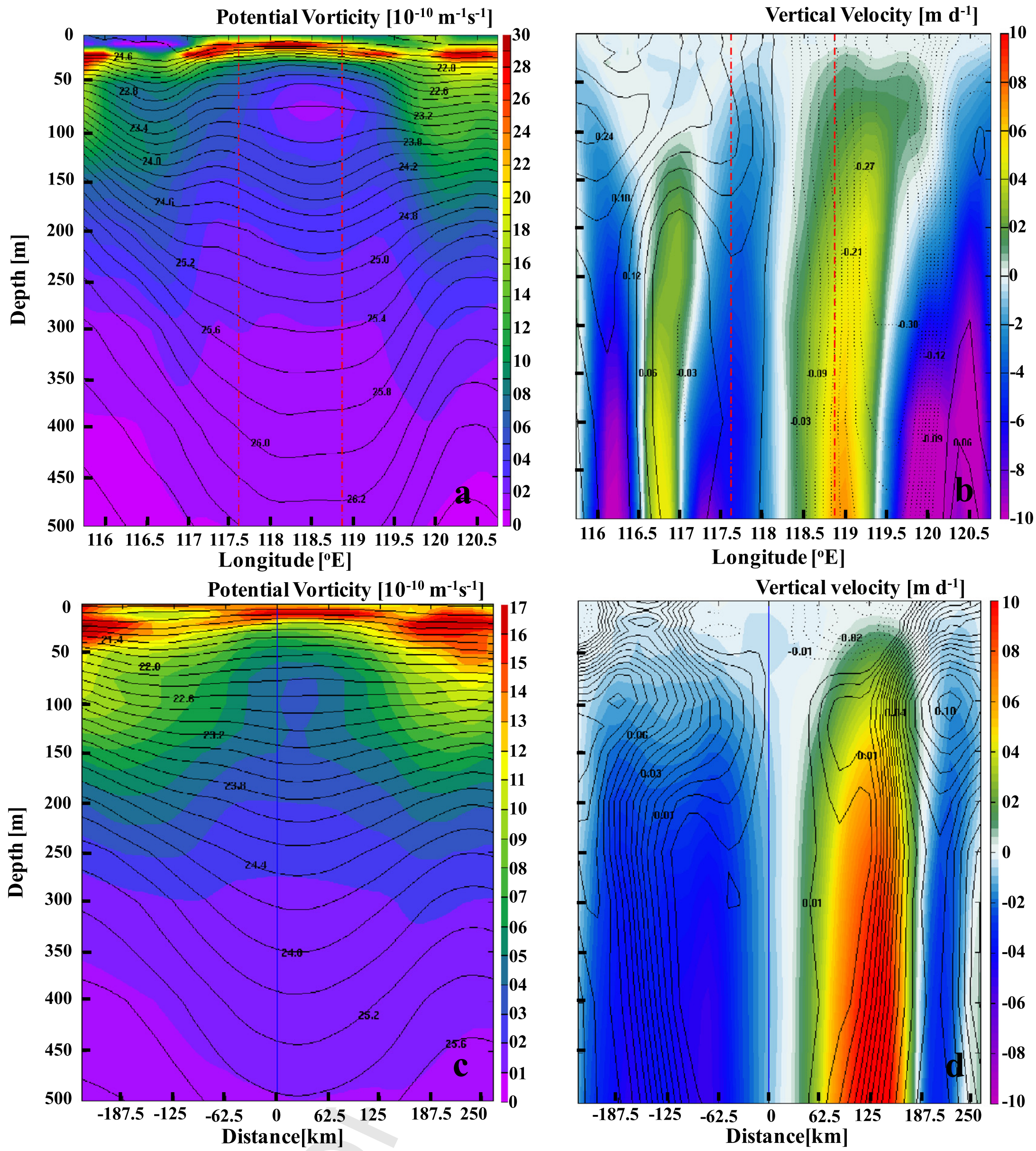

Fig. 8. Model-derived sectional distribution of potential vorticity (in 10^{-10} $m^{-1}\,s^{-1}$; isopycnals are also shown as contours) and vertical velocity (horizontal velocities in $m\,s^{-1}$ are denoted as contours; the flow directions are marked as solid and dashed lines). The upper panel is the potential vorticity and vertical velocity on 4 July 2007. (The boundaries of the eddy core are shown as red dashed lines.) The lower panel is the composite potential vorticity and vertical velocity during the entire lifetime of the anticyclonic eddy.

POC flux of 3.69 mmol C $m^{-2}\,d^{-1}$. This export level is still 1.6-fold higher than that for the reference stations.

To sum up the above discussion, a conceptual scheme of the biogeochemical responses coupled to physical dynamics within an anticyclonic eddy is proposed (Fig. 9). At the eddy edge, submesoscale upwelling first induces high nutrient influx into the upper euphotic zone and subsequently stimulates the phytoplankton growth rate and/or PP. We believe that the export events are delayed but then responsively enhanced, which would be reflected in high ^{234}Th removal fluxes. The upwelled water then converges towards the eddy center. The high export events superimposed on the water movement could ultimately lower the ^{234}Th activity in the eddy core.

5. Concluding remarks

We demonstrated that the 3D physical dynamics at submesoscales in anticyclonic eddies complicated the use of ^{234}Th to derive POC export fluxes in the ocean. In such eddy systems, any estimate of vertical export fluxes based on the 1D assumption at individual vertical horizons such as at eddy cores or at eddy edges could be misleading. Therefore, the oversimplified estimation based on eddy cores relative to reference sites to derive the suppression of POC export fluxes might have been biased.

Ideally, sampling at submesoscales of both the circulation field and ^{234}Th, along with other chemical parameters, to resolve the 3D structure of eddies is important for reliable estimation of the POC export associated with mesoscale eddies; however, this is not always possible in practice. Nevertheless, we contend that integration of eddy cores and edges would provide a first-order estimation of more accurate POC export fluxes.

Acknowledgements

We thank the Captain and Crew of the R/V *Dongfanghong II* for their assistance in sample collection during the cruise. We are

Please cite this article in press as: K. Zhou et al., Apparent enhancement of ^{234}Th-based particle export associated with anticyclonic eddies, Earth Planet. Sci. Lett. (2013), http://dx.doi.org/10.1016/j.epsl.2013.07.039

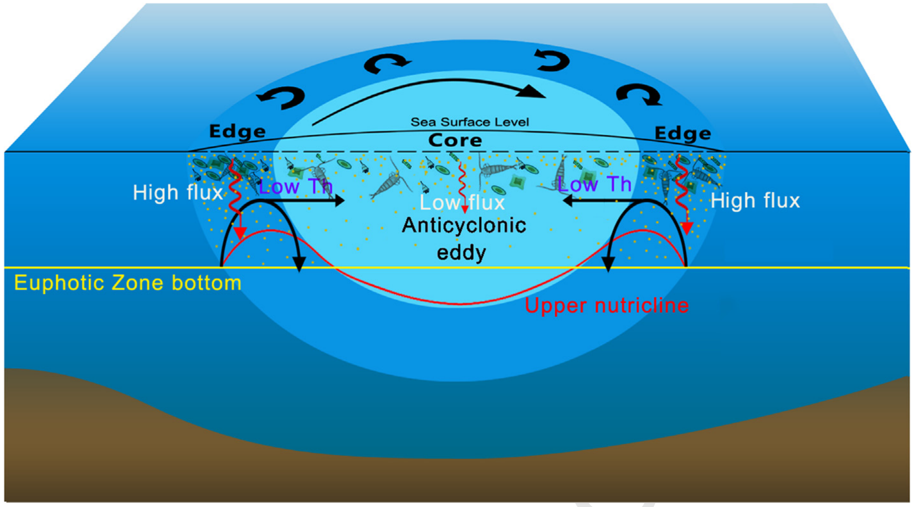

Fig. 9. Conceptual scheme of the biogeochemical responses coupled to physical dynamics within an anticyclonic eddy (constructed with inspiration from Mahadevan et al., 2008). At the eddy edge, the upper nutricline was uplifted into the euphotic zone (Ez) owing to submesoscale upwelling; the biological response was subsequently enhanced and higher particle export was expected to lower the ^{234}Th activity in the water column. In the eddy core, downward displacement of the upper nutricline prevented the nutrient from penetrating into the Ez, and no biological response or increase in particle export should be observed. However, the inward components of the velocity, induced by convergence of the surface water in the anticyclonic eddy, bring the water from the edge into the eddy core, which consequently lowers the ^{234}Th activity there. Therefore, ^{234}Th, $bSiO_2$ and POC fluxes observed in the eddy core were all enhanced relative to the reference stations.

grateful to Qian Liu for assistance with the sample collection and Zhenyu Sun for providing the SLA map. We also thank Xin Liu, Aiqin Han, and Lifang Wang for pigment and nutrient measurements. This work was supported by the National Basic Research Program of China (973 Program) through grant 2009CB421200, and by the National Natural Science Foundation of China (NSFC) through grants 41121091 and 41130857. The study also benefited from discussion with Dr. Ken Buesseler from Woods Hole Oceanographic Institution, who hosted K.Z. as a visiting student during March 2010–March 2011. Constructive comments from two anonymous reviewers and the editor greatly improved the quality of the paper. We thank Professor John Hodgkiss for assistance with English.

Appendix A. Supplementary material

Supplementary material related to this article can be found online at http://dx.doi.org/10.1016/j.epsl.2013.07.039.

Uncited references

(Buesseler et al., 1992) (Falkowski et al., 1991) (Hung et al., 2007) (Waples et al., 2006)

References

Benitez-Nelson, C.R., Bidigare, R.R., Dickey, T.D., Landry, M.R., Leonard, C.L., Nencioli, S.L.B.F., Rii, Y.M., Maiti, K., Becker, J.W., Bibby, T.S., Black, W., Cai, W.-J., Carlson, C.A., Chen, F., Kuwahara, V.S., Mahaffey, C., McAndrew, P.M., Quay, P.D., Rappé, M.S., Selph, K.E., Simmons, M.P., Yang, E.J., 2007. Mesoscale eddies drive increased silica export in the Subtropical Pacific Ocean. Science 316, 1017–1021.

Benitez-Nelson, C.R., Buesseler, K.O., Rutgers van der Loeff, M.M., Andrews, J., Ball, L., Crossin, G., Charette, M.A., 2001. Testing a new small-volume technique for determining ^{234}Th in seawater. J. Radioanal. Nucl. Chem. 248, 795–799.

Buesseler, K.O., Bacon, M.P., Cochran, J.K., Livingston, H.D., 1992. Carbon and nitrogen export during the JGOFS North Atlantic bloom experiment estimated from ^{234}Th:^{238}U disequilibria. Deep-Sea Res. 39, 1115–1137.

Buesseler, K.O., Benitez-Nelson, C.R., Rutgers van der Loeff, M.M., Andrews, J., Ball, L., Crossin, G., Charette, M.A., 2001. An intercomparison of small- and large-volume techniques for thorium-234 in seawater. Mar. Chem. 74, 15–28.

Buesseler, K.O., Benitez-Nelson, C.R., Moran, S.B., Burd, A., Charette, M., Cochran, J.K., Coppola, L., Fisher, N.S., Fowler, S.W., Gardner, W., Guo, L.D., Gustafsson, Ö., Lamborg, C., Masque, P., Miquel, J.C., Passow, U., Santschi, P.H., Savoye, N., Stewart, G., Trull, T., 2006. An assessment of particulate organic carbon to thorium-234 ratios in the ocean and their impact on the application of ^{234}Th as a POC flux proxy. Mar. Chem. 100, 213–233.

Buesseler, K.O., Lamborg, C., Cai, P.H., Escoube, R., Johnson, R., Pike, S., Masque, P., McGillicuddy, D.J., Verdeny, E., 2008. Particle fluxes associated with mesoscale eddies in the Sargasso Sea. Deep-Sea Res., Part 2 55, 1426–1444.

Cai, P.H., Chen, W.F., Dai, M.H., Wan, Z.W., Wang, D.X., Li, Q., Tang, T.T., Lv, D.W., 2008. A high-resolution study of particle export in the southern South China Sea based on ^{234}Th:^{238}U disequilibrium. J. Geophys. Res. 113, C04019.

Cai, P.H., Dai, M.H., Lv, D.W., Chen, W.F., 2006. An improvement in the small-volume technique for determining thorium-234 in seawater. Mar. Chem. 100, 282–288.

Cai, P.H., Rutgers van der Loeff, M.M., Stimac, I., Nöthig, E.-M., Lepore, K., Moran, S.B., 2010. Low export flux of particulate organic carbon in the central Arctic Ocean as revealed by ^{234}Th:^{238}U disequilibrium. J. Geophys. Res. 115, C10037.

Cao, Z.M., Dai, M.H., 2011. Shallow-depth $CaCO_3$ dissolution: Evidence from excess calcium in the South China Sea and its export to the Pacific Ocean. Glob. Biogeochem. Cycles 25, GB2019.

Chelton, D.B., Gaube, P., Schlax, M.G., Early, J.J., Samelson, R.M., 2011. The influence of nonlinear mesoscale eddies on near-surface oceanic chlorophyll. Science 334, 328–332.

Chen, J.H., Edwards, R.L., Wasserburg, G.J., 1986. ^{238}U, ^{234}U and ^{232}Th in seawater. Earth Planet. Sci. Lett. 80, 241–251.

Chen, W.F., 2008. On the export fluxes, seasonality and controls of particulate organic carbon in the Northern South China Sea. PhD dissertation. Xiamen University, China (in Chinese).

Chen, Y.-L.L., 2005. Spatial and seasonal variations of nitrate-based new production and primary production in the South China Sea. Deep-Sea Res., Part 1 52, 319–340.

Chen, Y.L.L., Chen, H.Y., Lin, I.I., Lee, M.A., Chang, J., 2007. Effects of cold eddy on phytoplankton production and assemblages in Luzon Strait bordering the South China Sea. J. Oceanogr. 63, 671–683.

Coale, K.H., Bruland, K.W., 1987. Oceanic stratified euphotic zone as elucidated by ^{234}Th:^{238}U disequilibria. Limnol. Oceanogr. 32, 189–200.

Du, C.J., Liu, Z.Y., Dai, M.H., Kao, S.-J., Cao, Z.M., Zhang, Y., Huang, T., Wang, L., Li, Y., 2013. Impact of the Kuroshio intrusion on the nutrient inventory in the upper northern South China Sea: insights from an isopycnal mixing model. Biogeosci. Discuss. 10, 6939–6972.

Falkowski, P.G., Ziemann, D., Kolber, Z., Bienfang, P.K., 1991. Role of eddy pumping in enhancing primary production in the ocean. Nature 352, 55–58.

Hansen, C., Kvaleberg, E., Samuelsen, A., 2010. Anticyclonic eddies in the Norwegian Sea: their generation, evolution and impact on primary production. Deep-Sea Res., Part 1 57, 1079–1091.

Hu, J.Y., Gan, J.P., Sun, Z.Y., Zhu, J., Dai, M.H., 2011. Observed three-dimensional structure of a cold eddy in the southwestern South China Sea. J. Geophys. Res. 116, C05016.

Hu, J.Y., Zheng, Q.A., Sun, Z.Y., Tai, C.-K., 2012. Penetration of nonlinear Rossby eddies into South China Sea evidenced by cruise data. J. Geophys. Res. 117, C03010.

Hung, J.J., Wang, S.M., Chen, Y.L., 2007. Biogeochemical controls on distributions and fluxes of dissolved and particulate organic carbon in the Northern South China Sea. Deep-Sea Res., Part 2 54, 1486–1503.

Klein, P., Lapeyre, G., 2009. The oceanic vertical pump induced by mesoscale and submesoscale turbulence. Annu. Rev. Mar. Sci. 1, 351–375.

Knap, A., Michaels, A., Close, A., Ducklow, H., Dickson, A., 1996. Protocols for the Joint Global Ocean Flux Study (JGOFS) core measurements. JGOFS Report No. 19 (reprint of the IOC Manuals and Guides 29, UNESCO 1994).
Lasternas, L., Piedeleu, M., Sangrá, P., Duarte, C.M., Agustí, S., 2012. Carbon fluxes forced by anticyclonic eddies generated by islands at the subtropical NE Atlantic Ocean. Biogeosci. Discuss. 9, 10241–10283.
Lin, I.-I., Lien, C.-C., Wu, C.-R., Wong, G.T.F., Huang, C.-W., Chiang, T.-L., 2010. Enhanced primary production in the oligotrophic South China Sea by eddy injection in spring. Geophys. Res. Lett. 37, L16602.
Liu, K.K., Chao, S.Y., Shaw, P.T., Gong, G.C., Chen, C.C., Tang, T.Y., 2002. Monsoon-forced chlorophyll distribution and primary production in the South China Sea: observations and a numerical study. Deep-Sea Res., Part 1 49, 1387–1412.
Liu, Y., Dai, M.H., Chen, W.F., Cao, Z.M., 2012. Distribution of biogenic silica in the upwelling zones in the South China Sea. Adv. Geosci. 28, 55–65.
Mahadevan, A., Thomas, L.N., Tandon, A., 2008. Comment on "Eddy/wind interactions stimulate extraordinary mid-ocean plankton blooms". Science 320, 448–449.
Maiti, K., Benitez-Nelson, C.R., Rii, Y., Bidigare, R., 2008. The influence of a mature cyclonic eddy on particle export in the lee of Hawaii. Deep-Sea Res., Part 2 55, 1445–1460.
McGillicuddy, D.J., Anderson, L.A., Bates, N.R., Bibby, T., Buesseler, K.O., Carlson, C.A., Davis, C.S., Ewart, C., Falkowski, P.G., Goldthwait, S.A., Hansell, D.A., Jenkins, W.J., Johnson, R., Kosnyrev, V.K., Ledwell, J.R., Li, Q.P., Siegel, D.A., Steinberg, D.K., 2007. Eddy/wind interactions stimulate extraordinary mid-ocean plankton blooms. Science 316, 1021–1026.
McGillicuddy, D.J., Robinson, A.R., Siegel, D.A., Jannasch, H.W., Johnson, R., Dickeys, T., McNeil, J., Michaels, A.F., Knap, A.H., 1998. Influence of mesoscale eddies on new production in the Sargasso Sea. Nature 394, 263–266.
Moutin, T., Prieur, L., 2012. Influence of anticyclonic eddies on the biogeochemistry from the oligotrophic to the ultraoligotrophic Mediterranean (BOUM cruise). Biogeosciences 9, 3827–3855.
Nan, F., He, Z.G., Zhou, H., Wang, D.X., 2011. Three long-lived anticyclonic eddies in the northern South China Sea. J. Geophys. Res. 116, C05002.
Olson, D.B., 1980. The physical oceanography of two rings observed by the cyclonic ring experiment, Part II: Dynamics. J. Phys. Oceanogr. 10, 514–528.
Oschlies, A., Garcon, V., 1998. Eddy-induced enhancement of primary production in a model of the north Atlantic Ocean. Nature 394, 266–269.
Ragueneau, O., Savoye, N., Del Amo, Y., Cotten, J., Tardiveau, B., Leynaert, A., 2005. A new method for the measurement of biogenic silica in suspended matter of coastal waters: using Si:Al ratios to correct for the mineral interference. Cont. Shelf Res. 25, 697–710.
Resplandy, L., Martin, A.P., Le Moigne, F., Martin, P., Aquilina, A., Mémery, L., Lévy, M., Sanders, R., 2012. How does dynamical spatial variability impact ^{234}Th-derived estimates of organic export? Deep-Sea Res., Part 1 68, 24–45.
Samuelsen, A., Hjøllo, S.S., Johannessen, J.A., Patel, R., 2012. Particle aggregation at the edges of anticyclonic eddies and implications for distribution of biomass. Ocean Sci. 8, 389–400.
Savoye, N., Benitez-Nelson, C., Burd, A.B., Cochran, J.K., Charette, M., Buesseler, K.O., Jackson, G.A., Roy-Barman, M., Schmidt, S., Elskens, M., 2006. ^{234}Th sorption and export models in the water column: a review. Mar. Chem. 100, 234–249.
Sweeney, E.N., McGillicuddy, D.J., Buesseler, K.O., 2003. Biogeochemical impacts due to mesoscale eddy activity in the Sargasso Sea as measured at the Bermuda Atlantic Time-series Study (BATS). Deep-Sea Res., Part 2 50, 3017–3039.
Wang, G.H., Su, J.L., Chu, P.C., 2003. Mesoscale eddies in the South China Sea observed with altimeter data. Geophys. Res. Lett. 30, 2121.
Waples, J.T., Benitez-Nelson, C., Savoye, N., Rutgers Van der Loeff, M.M., Baskaran, M., Gustafsson, Ö., 2006. An introduction to the application and future use of ^{234}Th in aquatic systems. Mar. Chem. 100, 166–189.
Xiu, P., Chai, F., Shi, L., Xue, H., Chao, Y., 2010. A census of eddy activities in the South China Sea during 1993–2007. J. Geophys. Res. 115, C03012.
Xiu, P., Chai, F., 2011. Modeled biogeochemical responses to mesoscale eddies in the South China Sea. J. Geophys. Res. 116, C10006.
Zhou, K.B., Nodder, S.D., Dai, M.H., Hall, J.A., 2012. Insignificant enhancement of export flux in the highly productive subtropical front, east of New Zealand: a high resolution study of particle export fluxes based on ^{234}Th:^{238}U disequilibria. Biogeosciences 9, 973–992.

XMLVIEW: extended

Appendix A. Supplementary material

The following is the Supplementary material related to this article.

begin ecomponent begin ecomponent begin ecomponent begin ecomponent begin ecomponent begin ecomponent begin ecomponent begin ecomponent begin ecomponent begin ecomponent begin ecomponent begin ecomponent begin ecomponent begin ecomponent begin ecomponent begin ecomponent begin ecomponent begin ecomponent

Label: MMC 1

caption: The supplementary material includes two parts. The first part was focused on the descriptions of the calculation of the surface geostrophic current and potential vorticity, the temporal evolution of the three anticyclonic eddies and comparison of nutrients, biomass and the phytoplankton community composition between the eddy cores, eddy edges and non-eddy references. The second part are five tables and three figures, they are respectively: **Table S1.** Temperature, salinity, particulate ^{234}Th, total ^{234}Th and ^{238}U activity, ^{234}Th/^{238}U ratio, POC, $bSiO_2$ and their ratios with particulate ^{234}Th in the northern South China Sea basin, measured in July–August 2007. **Table S2.** Inventories of total chlorophyll *a* (TChl *a*), fucoxanthin (Fuco), Particulate Organic Carbon (POC), biogenic silica ($bSiO_2$) and particulate ^{234}Th in the upper 100 m, POC/^{234}Th, $bSiO_2$/^{234}Th, steady-state ^{234}Th flux, POC flux and $bSiO_2$ flux at the depth of 100 m within the northern South China Sea basin in July–August 2007. **Table S3.** Responses of nutrients, community composition and biomass in eddy cores and eddy edges, and their comparisons with the reference stations outside the eddies. **Table S4.** Eigen values of PC1 and PC2 related with the individual parameters based on principal component analysis. Percentage of the variance explained by PC1 and PC2 is shown in parentheses. **Table S5.** Sea-level anomaly (SLA), surface salinity, Chl *a* at 75 m and the results from K-means cluster analysis for all core stations. **Fig. S1.** Relationship between Fuco and $bSiO_2$ in the northern South China Sea. **Fig. S2.** Correlation between particulate ^{234}Th and Chl *a*. **Fig. S3.** Correlation between in situ and MODIS Chl *a*.

link: **APPLICATION : mmc1**

end ecomponent end ecomponent end ecomponent end ecomponent end ecomponent end ecomponent end ecomponent end ecomponent end ecomponent end ecomponent end ecomponent end ecomponent end ecomponent end ecomponent end ecomponent end ecomponent end ecomponent end ecomponent end ecomponent

Highlights

- Low biomass/high 1D model-based ^{234}Th flux was seen in three anticyclonic cores.
- The enhancement of ^{234}Th flux in the eddy cores was apparent.
- We revealed dynamic exchanges between the eddy core and edge at the submesoscale.

Please cite this article in press as: K. Zhou et al., Apparent enhancement of ^{234}Th-based particle export associated with anticyclonic eddies, Earth Planet. Sci. Lett. (2013), http://dx.doi.org/10.1016/j.epsl.2013.07.039